

Article

Activated Carbons from Hydrothermal Carbonization and Chemical Activation of Olive Stones: Application in Sulfamethoxazole Adsorption

Elena Diaz ^{1,*} , Ines Sanchis ¹, Charles J. Coronella ² and Angel F. Mohedano ¹ 

¹ Chemical Engineering Department, Faculty of Sciences, Universidad Autonoma de Madrid, 28049 Madrid, Spain; ines.sanchis@uam.es (I.S.); angelf.mohedano@uam.es (A.F.M.)

² Department of Chemical and Materials Engineering, University of Nevada, Reno, NV 89557, USA; coronella@unr.edu

* Correspondence: elena.diaz@uam.es

Abstract: This work focuses on the production of activated carbons by hydrothermal carbonization of olive stones at 220 °C, followed by chemical activation with KOH, FeCl₃ and H₃PO₄ of the hydrochar obtained. In addition, N-doped hydrochars were also obtained by performing the hydrothermal carbonization process with the addition of (NH₄)₂SO₄. All hydrochars, N-doped and non-doped, showed low BET surface areas (4–18 m² g⁻¹). Activated hydrochars prepared using H₃PO₄ or KOH as activating agents presented BET surface areas of 1115 and 2122 m² g⁻¹, respectively, and those prepared from N-doped hydrochar showed BET surface area values between 1116 and 2048 m² g⁻¹ with an important contribution of mesoporosity (0.55–1.24 cm³ g⁻¹). The preparation procedure also derived inactivated hydrochars with predominantly acidic or basic groups on their surface. The resulting materials were tested in the adsorption of sulfamethoxazole in water. The adsorption capacity depended on both the porous texture and the electrostatic interactions between the adsorbent and the adsorbate. The adsorption equilibrium data (20 °C) fitted fairly well to the Langmuir equation, and even better to the Freundlich equation, resulting in the non-doped hydrochar activated with the KOH as the best adsorbent.

Keywords: activated carbon; adsorption; hydrochar; hydrothermal carbonization; N-doped materials; olive stones; sulfamethoxazole



Citation: Diaz, E.; Sanchis, I.; Coronella, C.J.; Mohedano, A.F. Activated Carbons from Hydrothermal Carbonization and Chemical Activation of Olive Stones: Application in Sulfamethoxazole Adsorption. *Resources* **2022**, *11*, 43. <https://doi.org/10.3390/resources11050043>

Academic Editor: Eveliina Repo

Received: 22 March 2022

Accepted: 24 April 2022

Published: 28 April 2022

Publisher's Note: MDPI stays neutral with regard to jurisdictional claims in published maps and institutional affiliations.



Copyright: © 2022 by the authors. Licensee MDPI, Basel, Switzerland. This article is an open access article distributed under the terms and conditions of the Creative Commons Attribution (CC BY) license (<https://creativecommons.org/licenses/by/4.0/>).

1. Introduction

Hydrothermal carbonization (HTC) is becoming an increasingly attractive way for the valorization of wet biomass wastes, which is carried out in the presence of water, at temperatures between 180 and 250 °C and the corresponding saturation pressure, and residence times between 5 min to 24 h [1–3]. The main reaction product is a solid known as hydrochar (HC), which is more stable and has a higher carbon content than the raw biomass. In addition, HTC produces a high organic loading of process water and a minimal gas fraction consisting mainly of CO₂. Hydrochar is commonly used: (i) for soil amendment [4]; (ii) as a source of energy [5–7]; or (iii) as a precursor of activated carbon materials [8–10]. In this sense, hydrothermal carbonization can be considered as a biomass pre-processing treatment to alter precursor properties prior to activation. HTC maintains the surface chemical functionality in the hydrochar and allows a more complete activation by favoring the development of a high porosity in the activation stage [11,12]. Physical activation consists of a high-temperature treatment (800–1100 °C) in a partially oxidizing atmosphere using steam, air or CO₂. Chemical activation requires the use of chemical reagents (KOH, ZnCl₂, K₂CO₃, H₃PO₄), a subsequent thermal treatment (usually 500–850 °C) for 1–24 h in an inert atmosphere and a final washing (usually with acid and water) to remove the excess activating agent [12–14]. As a result of the activation process, an increase in the

specific surface area of carbonaceous materials is achieved, which is more significant for chemical activation, and structural modifications and changes in their composition are also observed, such as the loss of oxygen functional groups or an increase in ash content [15].

Recently, N doping of hydrochar during the hydrothermal process has been used to modify the physical and chemical properties of hydrochar (e.g., increase in aromatic character, bulk N content, oxidation resistance and conductivity), without causing significant changes in the textural properties of hydrochar. Doped hydrochar requires an activation process to increase pore volume and surface area [16–20]. The incorporation of nitrogen into carbon structures has been shown to influence the performance of carbon materials used as energy-storage materials [21,22] and adsorbents [20,23–26]. Roldan et al. [20] prepared N-doped activated carbon by hydrothermal carbonization with ZnCl_2 as an activating agent (190 °C, 19 h) using glucose as a C precursor and pyrrole carboxaldehyde ($\text{C}_5\text{H}_5\text{NO}$) as a doping agent. They observed that the N-doped material showed higher mesoporosity (BET surface area (A_{BET}) = 503 $\text{m}^2 \text{g}^{-1}$, V_{mesopore} = 0.44 $\text{cm}^3 \text{g}^{-1}$, pore diameter = 12 nm, N = 3.9 wt.%) than the non-modified hydrochar (A_{BET} = 373 $\text{m}^2 \text{g}^{-1}$, V_{mesopore} = 0.14 $\text{cm}^3 \text{g}^{-1}$, pore diameter = 3.5 nm, N = 0 wt.%). This property was responsible for the higher adsorption capacity (q_e) of N-doped carbon (q_e = 159 mg g^{-1} methylene blue; q_e = 105 mg g^{-1} Rhodamine B) than the non-modified material (q_e = 88 mg g^{-1} methylene blue; q_e = 13 mg g^{-1} Rhodamine B). The porosity and N content of N-doped porous carbons can be tuned by adjusting the doping agent and C precursor ratio. In this regard, Huang et al. [26] prepared an N-doped carbon using NaNH_2 as a doping agent and a hydrochar from furfural. They doped the material with a NaNH_2 /hydrochar mass ratio of 2, 3 and 4 at 600 °C. The results showed an increase in porosity from 1068 to 2436 $\text{m}^2 \text{g}^{-1}$ with the ratio 2 (N = 0.78 wt.%) and 4 (N = 4.30 wt.%), achieving a CO_2 adsorption capacity (100 kPa and 0 °C) of 4.5 and 5.4 mmol g^{-1} , respectively.

For the preparation of low-cost adsorbents from biomass waste, both the amount of waste generated, and its location must be considered. Spain is the world's leading source of olives. The olive industry is an area of intensive agricultural activity and there are by-products that are not widely used and accumulate as waste. In the 2020–2021 campaign, 2.75 million hectares have been dedicated to achieving an olive production of 1.39 million tons [27]. Considering that the weight of the olive stone represents between 10–20 % of the total weight of the olive, the generation in this period of olive stones could exceed 200,000 tons. Olive stones are being widely used as fuel in southern Europe, especially in Croatia, Greece, Italy, Portugal, Slovenia, Spain and Turkey [28,29]. Recently, different alternatives have emerged to give value to this by-product as the production of catalysts [30], food supplements [31] and adsorbents for CO_2 removal [32,33], heavy metals [34,35], textile dyes [36] and pharmaceuticals [37,38]. Several preparation methods have been carried out to transform olive stones into a good adsorbent material. Moussa et al. [32,33] prepared activated carbon from olive stones by a first pyrolysis step (300 °C, 1 h, N_2) of the raw material, followed by KOH impregnation (85 °C, 3 h, KOH/OS mass ratio = 7) and a second pyrolysis step (350 °C, 2 h, N_2). They obtained activated carbons with an A_{BET} of 1345 $\text{m}^2 \text{g}^{-1}$, with an adsorption capacity of 5.7 mmol g^{-1} for CO_2 (0 °C, 1 bar), higher than those of other activated carbons prepared from algae (A_{BET} = 418 $\text{m}^2 \text{g}^{-1}$, q_e = 2.4 mmol g^{-1}) [39] or from empty fruit bunches of oil palms (A_{BET} = 2510 $\text{m}^2 \text{g}^{-1}$, q_e = 5.2 mmol g^{-1}) [40]. Bohli et al. [34] impregnated olive stones with H_3PO_4 (110 °C, 9 h) followed by a calcination process (380 °C, 2.5 h, N_2). They obtained an activated carbon characterized by an A_{BET} of 1194 $\text{m}^2 \text{g}^{-1}$ and a pH_{PZC} of 3.4, which was a good adsorbent to remove Cu (q_e = 17.7 mg g^{-1}), Cd (q_e = 57.1 mg g^{-1}) and Pb (q_e = 147.5 mg g^{-1}). These results were appreciably better than those obtained by other authors with apricot stones (A_{BET} = 566 $\text{m}^2 \text{g}^{-1}$, q_e = 24.1, 33.6 and 22.8 mg g^{-1} for Cu, Cd and Pb, respectively) [41]. The same preparation process was used by Limousy et al. [38] to prepare activated carbons for amoxicillin adsorption, obtaining a material (A_{BET} = 1174 $\text{m}^2 \text{g}^{-1}$) able to remove 93% of the antibiotic (20 °C for 25 mg L^{-1} initial concentration) with an adsorption capacity of 22.1 mg g^{-1} .

The aim of this work is the valorization of olive stones into activated carbon by means of hydrothermal carbonization and chemical activation of the resulting hydrochar. The effect of the N doping of the carbonaceous materials along the hydrothermal carbonization process on the characteristics of the adsorbent materials has been also studied. Hydrochars and activated hydrochars have been characterized by several techniques covering proximate and ultimate analyses, N₂ adsorption-desorption at 77 K, Scanning Electron Microscope (SEM) and pH_{slurry}. The potential of the activated hydrochars as adsorbents for the removal of pollutants in water has been tested using as a model compound an emerging pollutant, the sulfamethoxazole (SMX), a sulfonamide antibiotic used to treat urinary tract infections, bronchitis and prostatitis, which is effective against gram-negative and positive bacteria. That compound is frequently detected in wastewater and in drinking water at concentrations of 100–2500 ng L⁻¹ and 12 ng L⁻¹, respectively [42]. Table 1 collects some SMX adsorption results using non-commercial activated carbons from biomass wastes as adsorbents. The reported materials showed low specific surfaces, except those that follow preparation procedures based on the hydrothermal carbonization of biomass wastes and KOH chemical activation or pyrolysis at high temperatures. The results suggest that the electrostatic interaction between functionalized adsorbents and SMX plays an important role in pollutant removal.

Table 1. Summary of representative studies on sulfamethoxazole adsorption from water by biomass-derived adsorbents (the data correspond to the adsorbent that exhibits the best performance in each study).

Biomass Precursor	Adsorbent Preparation	Adsorbent Characteristics	Adsorption Conditions/Parameters	Ref.
Bagasse	Magnetic biochar prepared by FeCl ₃ impregnation and pyrolysis at 800 °C	C = 73.8% O = 21.8% N = 0.96% pH _{PZC} = 2.8 A _{BET} = 606 m ² g ⁻¹	SMX ₀ = 50 mg L ⁻¹ W = 0.2 g L ⁻¹ T = 25 °C pH = 5 q _L = 205 mg g ⁻¹	[43]
Dewatered waste activated sludge	Hydrothermal carbonization at 208 °C and KOH activation at 850 °C	C = 34.9% N = 5.8% pH _{slurry} = 5.5 A _{BET} = 832 m ² g ⁻¹	SMX ₀ = 25–175 mg L ⁻¹ W = 0.25 g L ⁻¹ T = 20 °C pH = 4.6 q _L = 423 mg g ⁻¹	[44]
Grape Seeds	Hydrothermal carbonization at 220 °C and KOH activation at 750 °C	C = 73.3% pH _{slurry} = 7.6 A _{BET} = 2194 m ² g ⁻¹	SMX ₀ = 25–150 mg L ⁻¹ W = 0.25 g L ⁻¹ T = 20 °C pH = 4.6 q _L = 650 mg g ⁻¹	[45]
Pine sawdust	Magnetic biochar prepared by FeCl ₂ , KOH and KNO ₃ impregnation at 90 °C	C = 55.8% O = 14.2% N < 0.3% pH _{PZC} = 9.5 A _{BET} = 126 m ² g ⁻¹	SMX ₀ = 0.5–9.0 mg L ⁻¹ W = 20 mg L ⁻¹ T = 25 °C pH = 4.5 q _L = 19.1 mg g ⁻¹	[46]
Bamboo	Thermal treatment (N ₂) at 380 °C and 2.5–10 psi followed by an activation with H ₃ PO ₄ at 600 °C	C = 52.0% O = 39.5% A _{BET} = 1.12 m ² g ⁻¹	SMX ₀ = 10 mg L ⁻¹ W = 100 mg L ⁻¹ T = 25 °C pH = 3.3 q _L = 88.1 mg g ⁻¹	[47]
Pine wood	Carbonization at 500 °C	C = 87.6% O = 12.2% A _{BET} = 328 m ² g ⁻¹	W = 0.45–0.68 mg L ⁻¹ Room temperature pH = 6 K _F = 131 n = 0.24	[48]

A_{BET}: specific surface area by Brunauer–Emmett–Teller (BET) equation; C: carbon content (wt.% d.b.); O: oxygen content (wt.% d.b.); N: nitrogen content (wt.% d.b.); Ash: ash content (wt.% d.b.); pH_{PZC}: pH at point of zero charge; SMX₀: initial sulfamethoxazole concentration; W: adsorbent dose; T: adsorption temperature; pH: adsorption pH; q_L: adsorption capacity from Langmuir model; K_F: Freundlich constant; n: adsorption intensity from Freundlich model.

2. Materials and Methods

2.1. Preparation of Hydrochars

Olive stones (OS), provided by a company located in Jaén (Spain), with an 18 wt.% of humidity and with a particle size of 5 mm were used as hydrochar precursors. In the first stage, the HTC process was carried out in a Teflon-lined stainless steel vessel (100 mL), using 20 g of dried olive stones and multiple water amounts to obtain an OS concentration in the reactor between 30–50 wt.% on a dry basis. The reactor was inserted in a muffle furnace (Hobersal series 8B Mod 12 PR/400) and heated up to 220 °C for 16 h [45]. The hydrochar was recovered by filtration, washed with distilled water and oven-dried at 105 °C for 24 h (Nabertherm R 60/750/12-C6).

Nitrogen doping of hydrochars was carried out using 20 g of dried OS and 50 wt.% water spiked with 7.9, 13.2 and 19.8 g of $(\text{NH}_4)_2\text{SO}_4$ (Panreac, 99%) in an initial C/N mass ratio of 5, 3 and 2, respectively [19]. HTC process and subsequent hydrochar washing were carried out under the same conditions abovementioned. Hydrochars were denoted as HC, followed by NX (HCNX) in cases of N-doped hydrochars, where X represents the initial C/N mass ratio.

2.2. Preparation of Activated Hydrochars

The hydrochar was physically mixed with the different activating agents, such as potassium hydroxide (KOH, Panreac, 85%), iron chloride (FeCl_3 , Panreac, 97%) or phosphoric acid (H_3PO_4 , Panreac, 85%) in a 3:1 mass ratio at room temperature. They were activated in a horizontal tube furnace (Nabertherm RHTH 120/300/18/C42) under a continuous N_2 flow (100 NmL min^{-1}). Activation with KOH and FeCl_3 was performed at 750 °C for 1 h with a heating rate of 10 °C min^{-1} [13,49,50]. In the case of H_3PO_4 , the mixture was left overnight at 60 °C and then heated at 500 °C (10 °C min^{-1} heating rate) for 2 h [51]. In addition, chemical activation with KOH, FeCl_3 and H_3PO_4 of the non-carbonized olive stones was carried out following the abovementioned procedure. In the cases of N-doped hydrochar, the activation process was carried out only with KOH under the same operating conditions. All activated materials were washed with 0.1 M HCl or NaOH and rinsed with deionized water to neutral pH. They were then recovered by filtration and finally dried at 105 °C overnight. The activated hydrochars were denoted, including the activating agent. For instance, HCN3-KOH represents the activated carbon obtained with KOH from the olive stone N-doped hydrochar with an initial mass ratio, C/N, of 3.

2.3. Characterization of Hydrochar and Activated Hydrochars

The proximate analyses were performed according to ASTM methods D3173-11 (moisture), D3174-11 (ash) and D3175-11 (volatile matter (VM)) using a Mettler Toledo apparatus (TGA/SDTA851e). The elemental analysis (C, N, S and H) was determined in a LECO Model CHNS-932 elemental analyzer. The analyses were performed in triplicate, with the standard deviation being less than 5% in all the cases.

N_2 adsorption-desorption isotherms at 77 K were performed in a Micromeritics apparatus (Tristar 3020). The samples were previously outgassed at 150 °C and a residual pressure of 10^{-3} Torr for 6 h in a Micromeritics VacPrep 061 device. The surface area was calculated by the BET equation and the micropore volume (V_{micro}) was obtained by the t-method. The difference between the volume of N_2 adsorbed at 0.95 relative pressure (as liquid) and the micropore volume was taken as the mesopore volume (V_{meso}).

Scanning Electron Microscope (SEM) images of the hydrochar and activated hydrochar samples were obtained in Hitachi S-3000N apparatus. The samples were metalized with gold using a Sputter Coater SC502. Images were obtained in the high vacuum mode under an accelerating voltage of 20 kV, using secondary and back-scattered electrons.

The $\text{pH}_{\text{slurry}}$ of the activated hydrochars was determined by measuring the pH (pH-meter, Crison) of an aqueous suspension of the sample (1 g) in deionized water (10 mL) after being stirred overnight [52].

2.4. Adsorption Tests

The potential application of activated hydrochar ($\approx 100 \mu\text{m}$ particle size) as an aqueous phase adsorbent was assessed using sulfamethoxazole (SMX) as a model compound. SMX has a solubility in water of 610 mg L^{-1} at 298 and a pKa of 1.7/5.6 [53]. Adsorption tests were performed by adding activated hydrochar (12.5 mg) into aqueous SMX solutions (25 to 300 mg L^{-1}) in 50 mL glass bottles. A commercial activated carbon (C: 89.5 wt.%, A_{BET} : $800 \text{ m}^2 \text{ g}^{-1}$; V_{micro} : $0.67 \text{ cm}^3 \text{ g}^{-1}$; V_{meso} : $0.53 \text{ cm}^3 \text{ g}^{-1}$; $\text{pH}_{\text{slurry}}$: 7.7), supplied by Merck, was used as a reference for comparison purposes. Experiments were carried out in a thermostated shaker bath (Optic Ivuyem System) at $20 \text{ }^\circ\text{C}$, 200 rpm and the natural pH of the SMX solution (4.6) for 72 h, which was more than enough time to reach equilibrium. SMX concentration was determined by UV-vis spectrophotometry (Cary 60 UV-Vis Agilent Technologies) at 265 nm. The reported results are the average values from triplicate runs, being the standard errors below 5%. Langmuir and Freundlich equations were used to fit the equilibrium data and parameters were calculated using Origin 9.1 software.

3. Results

3.1. Characterization of the Hydrochars and Activated Hydrochars

Table 2 shows the proximate and ultimate analyses of the feedstock and hydrochars. Elemental analysis indicates that the raw material has the typical mass composition of an olive stone: carbon (≈ 43 – 50 wt.%), oxygen (≈ 43 – 49 wt.%), hydrogen (≈ 6 – 7 wt.%) and low nitrogen and sulfur content (≤ 0.4 – 0.1 wt.%) [54–58]. In the case of non-doped hydrochar, the carbonization process led to an increase in C content (≈ 34 wt.%) and a decrease in oxygen (≈ 36 – 42 wt.%) and hydrogen (≈ 14 – 17 wt.%) content, because of the dehydration and decarboxylation reactions [59,60]. A reduced ash content (less than 0.8 wt.%) was observed in all cases. Regarding hydrochar yields, calculated as the mass of the hydrochar per unit mass of olive stone on a dry basis, values around 48–49 wt.% were obtained, regardless of the olive stone/water ratio (30–50 wt.% of OS on a dry basis) used in the HTC runs.

Table 2. Main characteristics of feedstock and hydrochars.

Sample	Biomass/ Water (wt.%)	Proximate Analysis (wt.% Dry Basis)			Ultimate Analysis (wt.% Dry Basis)					A_{BET} ($\text{m}^2 \text{ g}^{-1}$)
		Volatile Matter	Fixed Carbon	Ash	C	H	N	S	O *	
OS	-	77.2	22.4	0.4	49.9	5.8	0.1	0.1	43.7	-
HC	30	52.5	47.1	0.4	66.7	4.8	0.2	0.0	27.9	18
	40	57.0	42.2	0.8	67.8	5.0	0.2	0.1	26.1	17
	50	56.1	43.3	0.6	67.8	4.9	0.2	0.0	26.5	15
HCN2		64.7	35.0	0.3	54.0	4.8	7.7	6.4	26.8	5
HCN3	50	59.9	39.5	0.6	62.2	4.7	5.6	3.2	23.7	10
HCN5		60.5	39.1	0.4	63.9	4.9	4.9	1.4	24.5	4

* Calculated by difference $O = 100 - (C + H + N + S + \text{Ash})$.

N-doped hydrochars (HCN2, HCN3, HCN5) were prepared with an olive stones/water ratio of 50 wt.%, since it allows one to obtain a higher amount of hydrochar (Table 2). The C/N ratio in the initial solution (2, 3 and 5) was inferior to that of the hydrochar (7, 11 and 13) because of a less significant increase in carbon content than in nitrogen associated with the massive incorporation of nitrogen into the hydrochar structure, while no significant variations in the ash content were found. This fact has been observed previously in the literature using different nitrogen precursors ($(\text{NH}_4)_2\text{SO}_4$, $\text{C}_5\text{H}_5\text{NO}$, $\text{C}_2\text{H}_5\text{NO}_2$) [16,18,20]. Moreover, the use of $(\text{NH}_4)_2\text{SO}_4$ as a doping agent also provoked an increase in sulfur content in these hydrochars.

The N₂ adsorption-desorption isotherms at 77 K of the hydrochars (Figure 1) are associated with solids with low porosity. They showed very low adsorption at low relative pressures revealing a limited porosity in all cases with specific surface areas values in the range of 4–18 m² g⁻¹. The N-doped materials showed the lowest surface area values, below 10 m² g⁻¹, but with a significant contribution of mesoporosity. Table 3 summarizes the porous structure of the activated hydrochars. Representative N₂ adsorption-desorption isotherms are depicted in Figure 1. All of them correspond to essentially microporous solids with a higher contribution of mesoporosity for the HC-H₃PO₄ and N-doped materials. For comparison, the olive stones were also chemically activated, without hydrothermal carbonization treatment (Figure 1). The porous structure developed by these materials was much lower than that obtained from the hydrochars, achieving BET surface area values of 211, 504 and 254 m² g⁻¹ for olives stones activated with KOH, H₃PO₄ and FeCl₃, respectively, showing the crucial role of the HTC treatment in the development of the textural characteristics of activated hydrochars [44]. In the case of hydrochars, activation with FeCl₃ gave rise to a material with a relatively low surface area, slightly superior to the obtained by direct activation, while activation with H₃PO₄ resulted in a microporous material with a much higher relative contribution of mesoporosity, reaching BET surface area values of 1100 m² g⁻¹. Similar BET surface area values were obtained by direct activation of olive stones with steam, operating at 900 °C, a temperature significantly higher than those used in this work [61]. Activation with KOH allowed a high porosity development, essentially microporous, with BET surface area values up to around 2000 m² g⁻¹ and a significant ash content (17.1 wt.%). The activation treatments caused some important changes in the surface characteristics of the materials, specifically in the pH_{slurry} value. As described by other authors, activation with H₃PO₄ resulted in a material with an acidic surface, while activation with KOH led to a material with a more basic surface [13,62]. Finally, activation with FeCl₃ gave rise to an activated hydrochar with a slightly acidic surface.

Table 3. Main characteristics of feedstock and hydrochars.

Sample	C * (%)	N * (%)	Ash * (%)	A _{BET} (m ² g ⁻¹)	V _{micro} (cm ³ g ⁻¹)	V _{meso} (cm ³ g ⁻¹)	pH _{slurry}
HC-FeCl ₃	47.0	0.3	10.0	383	0.18	0.07	6.5
HC-H ₃ PO ₄	70.2	0.2	9.1	1155	0.50	0.20	1.8
HC-KOH	74.4	0.1	17.2	2122	0.96	0.14	8.0
HCN2-KOH	49.6	0.99	31.7	1247	0.13	0.60	2.3
HCN3-KOH	40.2	0.63	29.1	1116	0.21	0.55	2.8
HCN5-KOH	59.2	1.52	25.1	2048	0.86	1.24	4.2

* C, N and Ash are represented as wt.% dry basis.

The potential of KOH as an activating agent was also tested in the activation of N-doped hydrochar, giving rise to materials with high surface area (1100–2000 m² g⁻¹), but significantly lower than that shown by the HC-KOH activated hydrochar, especially in the cases where the initial C/N mass ratio was lower (HCN2 and HCN3). This fact is related to the high ash content of these materials since the BET surface area represents up to about 1574–2734 m² g⁻¹ on an ash-free basis. Regarding pore size, the high N content in the precursor material favored the synthesis of mesoporous activated carbons [20]. The C/N ratio increased significantly after the activation treatment, indicating that the high temperature of the activation process caused the transformation of N into volatile N compounds leading to the loss of surface functional groups and resulting in the production of more stable N-containing species in the carbonaceous structure [63].

As previously discussed, the activation treatment causes some changes in the pH_{slurry} of the activated hydrochars (Table 3). In the case of the N-doped hydrochars, the low values of pH_{slurry} (2.3–4.8), despite being activated with KOH, could be attributed to the N-doping

agent ($(\text{NH}_4)_2\text{SO}_4$) causing a modification of oxygen groups leading to an increase in carboxylic acids [18].

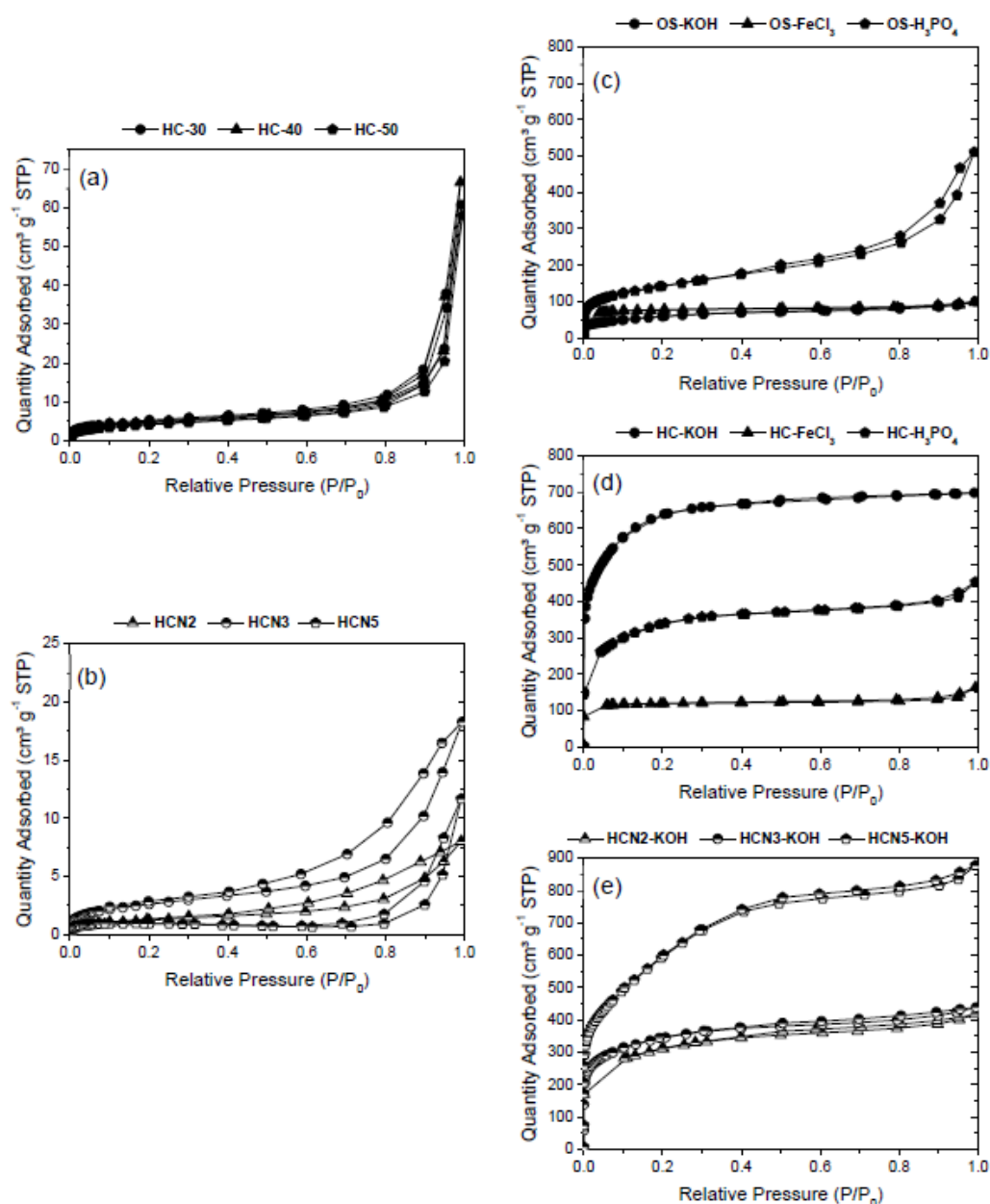


Figure 1. N_2 adsorption-desorption isotherms at 77 K of (a) hydrochar obtained at different biomass/water ratio (30–50 wt.%), (b) N-doped hydrochar, (c) materials obtained by direct activation of olive stones, (d) activated hydrochar and (e) activated N-doped hydrochar.

Figure 2 shows the scanning electron micrographs (SEM) of the surface of the olive stones, hydrochars and activated hydrochars. The raw olive stones presented a well-defined and regular structure, while the hydrochars showed some partial degradation of the surface, maintaining their original morphology, indicating the good thermo-mechanical stability of the raw material. The N-doped hydrochars showed multiple spheres of 1–5 μm diameter over the surface, originating in the doping process with $(\text{NH}_4)_2\text{SO}_4$. From the hydrochar images, non-porous materials were observed. However, activated hydrochars showed high porosity, with different structures depending on the activating agent. The hydrochars activated with KOH (HC-KOH and HCN5-KOH) showed cavities and cracks on their external surface, more regular in the case of the non-doped material. In the case of

FeCl_3 -activation, the formation of microspheres was observed, while after activation with H_3PO_4 , prismatic particles can also be seen.

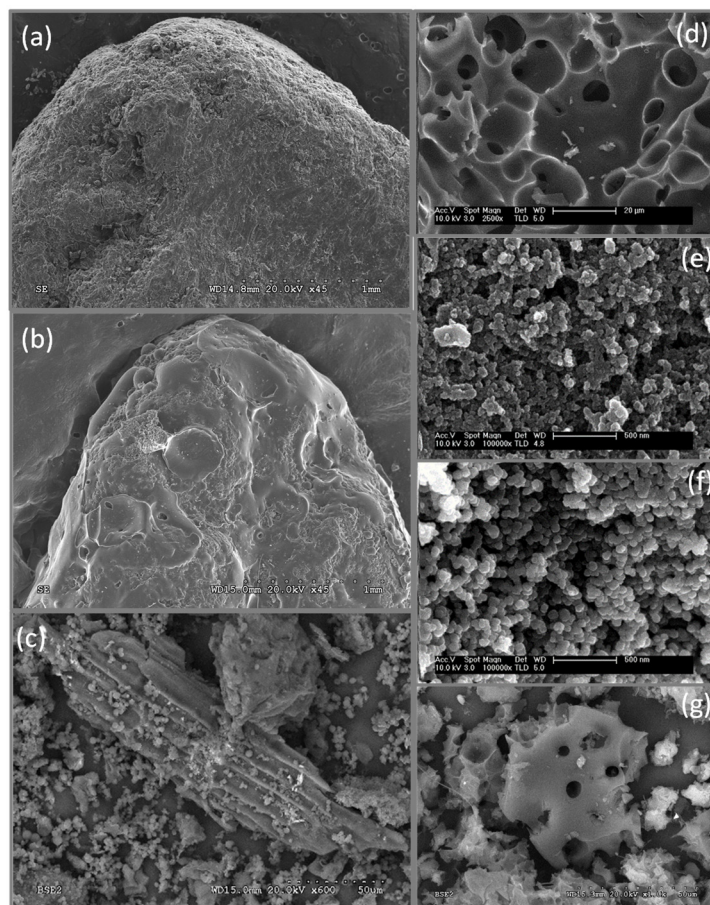


Figure 2. SEM images of (a) OS, (b) HC-50, (c) HCN5, (d) HC-KOH, (e) HC- FeCl_3 , (f) HC- H_3PO_4 and (g) HCN5-KOH.

3.2. Adsorption of Sulfamethoxazole

The activated hydrochars were used in the SMX adsorption experiments, together with a commercial activated carbon, whose main characteristics were included in Section 2.4. for comparison purposes. Figure 3 shows the adsorption isotherms at 20 °C. The experimental data were fitted to the Langmuir (1) and Freundlich (2) equations:

$$q_e = \frac{q_L \cdot K_L \cdot C_e}{1 + K_L \cdot C_e} \quad (1)$$

$$q_e = K_F \cdot C_e^{\frac{1}{n}} \quad (2)$$

where q_e is the equilibrium adsorbate loading onto the adsorbent (mg g^{-1}); C_e , the equilibrium liquid phase concentration of adsorbate (mg L^{-1}); q_L , the monolayer adsorption capacity of the material (mg g^{-1}); K_L , the Langmuir constant (L mg^{-1}); K_F , the Freundlich constant ($(\text{mg g}^{-1}) \cdot (\text{L mg}^{-1})^{(1/n)}$) and n is the adsorption intensity. The values of the fitting parameters and correlation coefficients are given in Table 4. As can be seen, the results fitted the Freundlich equation better than the Langmuir equation, especially in the case of the adsorbents from HC. The HC-KOH material showed the highest adsorption capacity of the Langmuir monolayer, reaching almost the value of 760 mg g^{-1} , followed by the materials obtained by KOH activation of N-doped hydrochars (q_L : $429\text{--}695 \text{ mg g}^{-1}$). These adsorption capacity values are comparable to or even superior to those obtained with

adsorbents prepared from other biomass wastes (Table 1). Regarding Freundlich isotherms, the value of the “ n ” was lower than 1 (0.17–0.33) associated with favorable isotherms, with a high amount of adsorbate adsorbed at low concentrations [64]. Except in the case of the HC-H₃PO₄ material, values of “ n ” were between 0.17 and 0.22, so an approximation of the adsorption capacity of the materials could be established from “ K_F ” values with the following sequence: HC-KOH > HCN5-KOH > HCN2-KOH > HCN3-KOH >> commercial AC > HC-FeCl₃. Attending to the value of “ q_L ”, calculated from the Langmuir equation, the resultant sequence would be the same, placing HC-H₃PO₄ between HCN3-KOH and commercial AC.

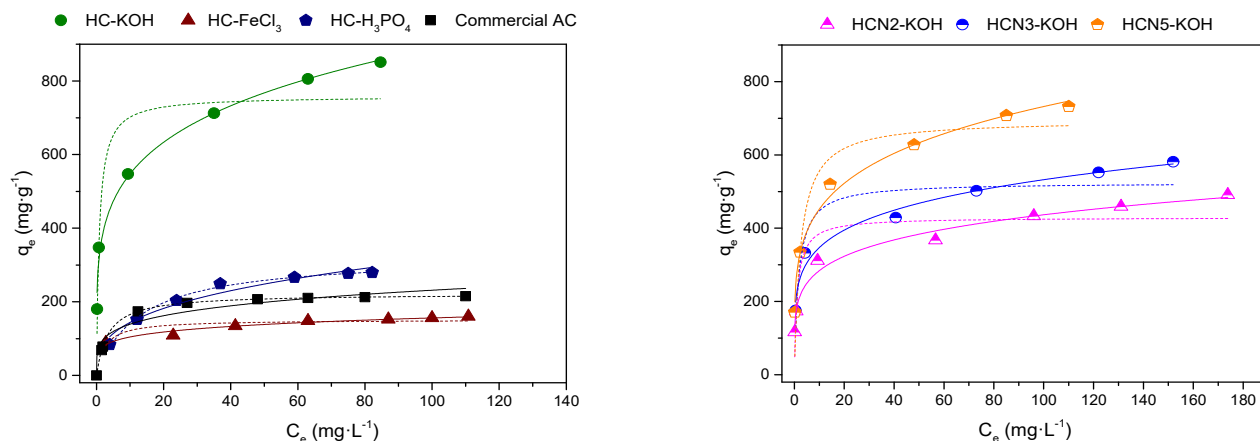


Figure 3. Adsorption isotherms of SMX on HC-KOH, HC-FeCl₃, HC-H₃PO₄, HCN2-KOH, HCN3-KOH and HCN5-KOH and commercial activated carbon at 20 °C (symbols: experimental values; short dot lines: fitting to the Langmuir equation; solid lines: fitting to the Freundlich equation).

Table 4. Langmuir and Freundlich parameters for SMX adsorption on the activated carbons of Figure 3.

Sample	Langmuir			Freundlich		
	q_L (mg g ⁻¹)	K_L (L mg ⁻¹)	R^2	K_F (mg g ⁻¹) · (L mg ⁻¹) ^(1/n)	n	R^2
Commercial AC	221.8 ± 9.2	0.296 ± 0.071	0.951	83.8 ± 12.1	0.220 ± 0.036	0.938
HC-FeCl ₃	151.2 ± 7.6	0.419 ± 0.187	0.673	69.9 ± 5.7	0.174 ± 0.019	0.945
HC-H ₃ PO ₄	324.4 ± 7.4	0.078 ± 0.007	0.992	66.3 ± 10.4	0.337 ± 0.039	0.947
HC-KOH	758.7 ± 55.9	1.236 ± 0.630	0.855	338.3 ± 18.3	0.209 ± 0.014	0.987
HCN2-KOH	524.6 ± 34.2	0.579 ± 0.290	0.830	226.2 ± 16.8	0.186 ± 0.017	0.975
HCN3-KOH	429.4 ± 29.3	0.862 ± 0.464	0.829	184.8 ± 11.5	0.187 ± 0.014	0.982
HCN5-KOH	695.4 ± 48.9	0.397 ± 0.185	0.878	278.9 ± 14.6	0.209 ± 0.013	0.989

The adsorption capacity of the activated hydrochars was mainly influenced by the BET surface area of the carbons followed by the existence of acid or basic surface functional groups. This fact was also observed in the adsorption of methylene blue using KOH-modified hydrochar from sewage sludge, where the adsorption process was the result of several phenomena such as physi- and chemisorption, acid-base and redox equilibria [65]. In this study, consistently with their much larger surface area, HC-KOH and HCN5-KOH yielded the highest adsorption capacity. Comparing these two materials, electrostatic interactions could explain the best performance of the HC-KOH material. At solution pH (4.6), SMX should be mostly a neutral and anionic species. Since the pH_{slurry} of HCN5-KOH is 4.2, its surface will be negatively charged, while the surface of the HC-KOH

material will be positively charged, which will favor the interaction of the latter with the adsorbent [45,66,67]. Then, the effect of N doping did not have a positive effect on the adsorption of the SMX to provide positively charged functional groups on the surface of the adsorbent. A comparison of the adsorption capacity of HC-H₃PO₄, HCN2-KOH, HCN3-KOH materials, which are characterized by similar values of specific surface area (A_{BET} : 1115–1247 m² g⁻¹) and pH_{slurry} lower than that of the solution, allows the evaluation of the effect of acidic or basic functional groups on the surface of the activated hydrochars on the adsorption capacity of SMX. The better performance of the N-doped materials, with similar properties to the HC-H₃PO₄ activated hydrochar could be attributed to the higher negative charge of the latter, whose pH_{slurry} is like pKa 1 of SMX. Finally, the substantial differences in adsorption capacity between the HC-FeCl₃ and HC-H₃PO₄ materials, and the commercial AC, used as reference material, could be due to the lower surface area of the former since all of them present similar electrostatic interactions with the adsorbate.

4. Conclusions

Hydrothermal carbonization followed by chemical activation with KOH of olive stones can be a promising way of valorization of such biomass to produce activated hydrochars. Activation with FeCl₃, H₃PO₄ and KOH of hydrochar resulted in high BET surface area carbons with predominantly microporous structure and a neutral, acidic and basic surface, while KOH activation of N-doped hydrochar also provided activated carbons with a high BET surface area but with a significant contribution of mesoporosity and an acidic surface. These activated hydrochars can be used as adsorbents for pollutants in water, as can be deduced from the high adsorption capacity shown for sulfamethoxazole, based on the high BET area value and the electrostatic interaction between the adsorbent and the adsorbate.

Author Contributions: Conceptualization, E.D., C.J.C., A.F.M.; Methodology, E.D., I.S.; Investigation, E.D., I.S.; Writing—Original Draft Preparation, E.D., I.S., A.F.M.; Writing—Review and Editing, E.D., C.J.C., A.F.M.; Supervision, E.D., C.J.C., A.F.M.; Funding Acquisition, E.D., C.J.C., A.F.M. All authors have read and agreed to the published version of the manuscript.

Funding: The authors greatly appreciate the financial support from the Spanish MICIIN (PID 2019-108445RB-I00), Comunidad de Madrid (S2018/EMT-4344), US National Science Foundation (NSF #CBET-1856009), and UAM-Santander (2017/EEUU/07). I. Sanchis wishes to thank the Comunidad de Madrid for PEJD-2017-PRE/AMB-4616 contract.

Institutional Review Board Statement: Not applicable.

Informed Consent Statement: Not applicable.

Data Availability Statement: Not applicable.

Acknowledgments: The authors thank F.J. Manzano for his valuable help.

Conflicts of Interest: The authors declare no conflict of interest.

References

1. Ischia, G.; Fiori, L. Hydrothermal carbonization of organic waste and biomass: A review on process, reactor, and plant modelling. *Waste Biomass Valorization* **2021**, *12*, 2797–2824. [[CrossRef](#)]
2. Marzbali, M.H.; Kundu, S.; Halder, P.; Patel, S.; Hakeem, I.G.; Paz-Ferreiro, J.; Madapusi, S.; Surapaneni, A.; Shah, K. Wet organic waste treatment via hydrothermal processing: A critical review. *Chemosphere* **2021**, *279*, 130557. [[CrossRef](#)]
3. Zhang, Z.; Yang, J.; Qian, J.; Zhao, Y.; Wang, T.; Zhai, Y. Biowaste hydrothermal carbonization for hydrochar valorization: Skeleton structure, conversion pathways and clean biofuel applications. *Bioresour. Technol.* **2021**, *324*, 124686. [[CrossRef](#)]
4. Mau, V.; Arye, G.; Gross, A. Poultry litter hydrochar as an amendment for sandy soils. *J. Environ. Manag.* **2020**, *271*, 110959. [[CrossRef](#)]
5. Bardhan, M.; Novera, T.M.; Tabassum, M.; Islam, M.A.; Islam, M.A.; Hameed, B.H. Co-hydrothermal carbonization of different feedstocks to hydrochar as potential energy for the future world: A review. *J. Clean. Prod.* **2021**, *298*, 126734. [[CrossRef](#)]
6. Wu, L.; Wei, W.; Wang, D.; Ni, B.J. Improving nutrients removal and energy recovery from wastes using hydrochar. *Sci. Total Environ.* **2021**, *783*, 146980. [[CrossRef](#)]

7. Lang, J.; Matějová, L.; Cuentas-Gallegos, A.K.; Lobato-Peralta, D.R.; Ainassaari, K.; Gómez, M.M.; Solís, J.L.; Mondal, D.; Keiski, R.L.; Cruz, G.J.F. Evaluation and selection of biochars and hydrochars derived from agricultural wastes for the use as adsorbent and energy storage materials. *J. Environ. Chem. Eng.* **2021**, *9*, 105979. [[CrossRef](#)]
8. Hou, Z.; Tao, Y.; Bai, T.; Liang, Y.; Huang, S.; Cai, J. Efficient Rhodamine B removal by N-doped hierarchical carbons obtained from KOH activation and urea-oxidation of glucose hydrochar. *J. Environ. Chem. Eng.* **2021**, *9*, 105757. [[CrossRef](#)]
9. Tu, W.; Liu, Y.; Xie, Z.; Chen, M.; Ma, L.; Du, G.; Zhu, M. A novel activation-hydrochar via hydrothermal carbonization and KOH activation of sewage sludge and coconut shell for biomass wastes: Preparation, characterization and adsorption properties. *J. Colloid Interface Sci.* **2021**, *593*, 390–407. [[CrossRef](#)]
10. Zubbri, N.A.; Mohamed, A.R.; Lahijani, P.; Mohammadi, M. Low temperature CO₂ capture on biomass-derived KOH-activated hydrochar established through hydrothermal carbonization with water-soaking pre-treatment. *J. Environ. Chem. Eng.* **2021**, *9*, 105074. [[CrossRef](#)]
11. Diao, Y.; Walawender, W.P.; Fan, L.T. Activated carbons prepared from phosphoric acid activation of grain sorghum. *Bioresour. Technol.* **2002**, *81*, 45–52. [[CrossRef](#)]
12. MacDermid-Watts, K.; Adewakun, E.; Abhi, T.D.; Pradhan, R.; Dutta, A. Hydrothermal carbonization valorization as an alternative application for corn bio-ethanol by-products. *J. Environ. Chem. Eng.* **2021**, *9*, 105431. [[CrossRef](#)]
13. Bedia, J.; Peñas-Garzón, M.; Gómez-Avilés, A.; Rodriguez, J.J.; Belver, C. A review on the synthesis and characterization of biomass-derived carbons for adsorption of emerging contaminants from water. *J. Carbon Res.* **2018**, *4*, 63. [[CrossRef](#)]
14. Patra, B.R.; Mukherjee, A.; Nanda, S.; Dalai, A.K. Biochar production, activation and adsorptive applications: A review. *Environ. Chem. Lett.* **2021**, *19*, 2237–2259. [[CrossRef](#)]
15. Yaah, V.B.K.; Zbair, M.; de Oliveira, S.B.; Ojala, S. Hydrochar-derived adsorbent for the removal of diclofenac from aqueous solution. *Nanotechnol. Environ. Eng.* **2021**, *6*, 3. [[CrossRef](#)]
16. Baccile, N.; Laurent, G.; Coelho, C.; Babonneau, F.; Zhao, L.; Titirici, M.M. Structural insights on nitrogen-containing hydrothermal carbon using solid-state magic angle spinning ¹³C and ¹⁵N nuclear magnetic resonance. *J. Phys. Chem. C* **2011**, *115*, 8976–8982. [[CrossRef](#)]
17. Falco, C.; Sevilla, M.; White, R.J.; Rothe, R.; Titirici, M.M. Renewable nitrogen-doped hydrothermal carbons derived from microalgae. *ChemSusChem* **2012**, *5*, 1834–1840. [[CrossRef](#)]
18. Latham, K.G.; Jambu, G.; Joseph, S.D.; Donne, S.W. Nitrogen doping of hydrochars produced hydrothermal treatment of sucrose in H₂O, H₂SO₄, and NaOH. *ACS Sustain. Chem. Eng.* **2014**, *2*, 755–764. [[CrossRef](#)]
19. Latham, K.G.; Dose, W.M.; Allen, J.A.; Donne, S.W. Nitrogen doped heat treated and activated hydrothermal carbon: NEXAFS examination of the carbon surface at different temperatures. *Carbon* **2018**, *128*, 179–190. [[CrossRef](#)]
20. Roldan, L.; Marco, Y.; García-Bordeje, E. Bio-sourced mesoporous carbon doped with heteroatoms (N,S) synthesised using one-step hydrothermal process for water remediation. *Microporous Mesoporous Mater.* **2016**, *222*, 55–62. [[CrossRef](#)]
21. Chen, P.; Yang, J.J.; Li, S.S.; Wang, Z.; Xiao, T.Y.; Qian, Y.H.; Yu, S.H. Hydrothermal synthesis of macroscopic nitrogen-doped graphene hydrogels for ultrafast supercapacitor. *Nano Energy* **2013**, *2*, 249–256. [[CrossRef](#)]
22. Zhang, X.; Zhu, G.; Wang, M.; Li, J.; Lu, T.; Pan, L. Covalent-organic-frameworks derived N-doped porous carbon materials as anode for superior long-life cycling lithium and sodium ion batteries. *Carbon* **2017**, *116*, 686–694. [[CrossRef](#)]
23. Horikawa, T.; Sakao, N.; Sekida, T.; Hayashi, J.; Do, D.D.; Katoh, M. Preparation of nitrogen-doped porous carbon by ammonia gas treatment and the effects of N-doping on water adsorption. *Carbon* **2012**, *50*, 1833–1842. [[CrossRef](#)]
24. Gu, J.M.; Kim, W.S.; Hwang, Y.K.; Huh, S. Template-free synthesis of N-doped porous carbons and their gas sorption properties. *Carbon* **2013**, *56*, 208–217. [[CrossRef](#)]
25. Bai, F.; Xia, Y.; Chen, B.; Su, H.; Zhu, Y. Preparation and carbon dioxide uptake capacity of N-doped porous carbon materials derived from direct carbonization of zeolitic imidazolate framework. *Carbon* **2014**, *79*, 213–226. [[CrossRef](#)]
26. Huang, K.; Li, Z.L.; Zhang, J.Y.; Tao, D.J.; Liu, F.; Dai, S. Simultaneous activation and N-doping of hydrothermal carbons by NaNH₂: An effective approach to CO₂ adsorbents. *J. CO₂ Util.* **2019**, *33*, 405–412. [[CrossRef](#)]
27. Datos Mensuales de Producción, Movimiento y Existencias (AICA), Ministerio de Agricultura, Pesca y Alimentación. Available online: https://www.mapa.gob.es/es/agricultura/temas/producciones-agricolas/aceite-oliva-y-aceituna-mesa/Datos_produccion_movimiento_existencias_AICA.aspx (accessed on 28 February 2022).
28. Rukavina, H.; Furlan, M.; Karampinis, E.; Margaritis, N.; Panagiotis, V.; Bau, L.; Francescato, V.; Almeida, T.; Figo, S.; Scap, S.; et al. Developing the Sustainable Market of Residential Mediterranean Solid Biofuels. BIOmasudplus. 2017. Available online: <https://cordis.europa.eu/project/id/691763> (accessed on 23 April 2022).
29. Mediavilla, I.; Barro, R.; Borjabad, E.; Peña, D.; Fernández, M.J. Quality of olive stone as a fuel: Influence of oil content on combustion process. *Renew. Energy* **2020**, *160*, 374–384. [[CrossRef](#)]
30. Mahmoudi, M.; Dentzer, J.; Gadiou, R.; Ouederni, A. Evaluation of activated carbons based on olive stones as catalysts during hydrogen production by thermocatalytic decomposition of methane. *Int. J. Hydrogen Energy* **2017**, *42*, 8712–8720. [[CrossRef](#)]
31. Bolek, S. Olive stone powder: A potential source of fiber and antioxidant and its effect on the rheological characteristics of biscuit dough and quality. *Innov. Food Sci. Emerg. Technol.* **2020**, *64*, 102423. [[CrossRef](#)]
32. Moussa, M.; Bader, N.; Querejeta, N.; Durán, I.; Pevida, C.; Ouederni, A. Toward sustainable hydrogen storage and carbon dioxide capture in post-combustion conditions. *J. Environ. Chem. Eng.* **2017**, *5*, 1628–1637. [[CrossRef](#)]

33. Moussa, M.; Bader, N.; Querejeta, N.; Duran, I.; Pevida, C.; Ouederni, A. CO₂ adsorption on activated carbon based olive stone: A comparison of Langmuir and Freundlich models. In *Recent Advances in Environmental Science from the Euro-Mediterranean and Surrounding Regions (EMCEI 2017)*; Springer: Berlin/Heidelberg, Germany, 2018; pp. 1099–1100. [[CrossRef](#)]
34. Bohli, T.; Ouederni, A.; Fiol, N.; Villaescusa, I. Evaluation of an activated carbon from olive stones used as an adsorbent for heavy metal removal from aqueous phases. *C. R. Chim.* **2015**, *18*, 88–99. [[CrossRef](#)]
35. Corral-Bobadilla, M.; Lostado-Lorza, R.; Somovilla-Gomez, F.; Escribano-García, R. Effective use of activated carbon from olive stone waste in the biosorption removal of Fe (III) ions from aqueous solutions. *J. Clean. Prod.* **2021**, *294*, 126332. [[CrossRef](#)]
36. Al-Ghouti, M.A.; Sweleh, A.O. Optimizing textile dye removal by activated carbon prepared from olive stones. *Environ. Technol. Innov.* **2013**, *16*, 100488. [[CrossRef](#)]
37. Larous, S.; Meniai, A.H. Adsorption of Diclofenac from aqueous solution using activated carbon prepared from olive stones. *Int. J. Hydrogen Energy* **2016**, *41*, 10380–10390. [[CrossRef](#)]
38. Limousy, L.; Ghouma, I.; Ouederni, A.; Jeguirim, M. Amoxicillin removal from aqueous solution using activated carbon prepared by chemical activation of olive stone. *Environ. Sci. Pollut. Res.* **2017**, *24*, 9993–10004. [[CrossRef](#)]
39. Zhang, Z.; Wang, K.; Atkinson, J.D.; Yan, X.; Li, X.; Rood, M.J.; Yan, Z. Sustainable and hierarchical porous Enteromorpha prolifera based carbon for CO₂ capture. *J. Hazard. Mater.* **2012**, *229–230*, 183–191. [[CrossRef](#)]
40. Parshetti, G.K.; Chowdhury, S.; Balasubramanian, R. Biomass derived low-cost microporous adsorbents for efficient CO₂ capture. *Fuel* **2015**, *148*, 246–254. [[CrossRef](#)]
41. Kobya, M.; Demirbas, E.; Senturk, E.; Ince, M. Adsorption of heavy metal ions from aqueous solutions by activated carbon prepared from apricot stone. *Bioresour. Technol.* **2005**, *96*, 1518–1521. [[CrossRef](#)]
42. Kumar, A.; Sharma, S.K.; Sharma, G.; Guo, C.; Vo, D.V.N.; Iqbal, J.; Naushad, M.; Stadler, F.J. Silicate glass matrix@Cu₂O/Cu₂V₂O₇ p-n heterojunction for enhanced visible light photo-degradation of sulfamethoxazole: High charge separation and interfacial transfer. *J. Hazard. Mater.* **2021**, *402*, 123790. [[CrossRef](#)]
43. Zhang, R.; Zheng, X.; Chen, B.; Ma, J.; Niu, X.; Zhang, D.; Lin, Z.; Fu, M.; Zhou, S. Enhanced adsorption of sulfamethoxazole from aqueous solution by Fe-impregnated graphited biochar. *J. Clean. Prod.* **2020**, *256*, 120662. [[CrossRef](#)]
44. Villamil, J.A.; Diaz, E.; de la Rubia, M.A.; Mohedano, A.F. Potential use of waste activated sludge hydrothermally treated as a renewable fuel or activated carbon precursor. *Molecules* **2020**, *25*, 3534. [[CrossRef](#)] [[PubMed](#)]
45. Diaz, E.; Manzano, F.J.; Villamil, J.; Rodriguez, J.J.; Mohedano, A.F. Low-cost activated grape seed-derived hydrochar through hydrothermal carbonization and chemical activation for sulfamethoxazole adsorption. *Appl. Sci.* **2019**, *9*, 5127. [[CrossRef](#)]
46. Reguyal, F.; Sarmah, A.K. Adsorption of sulfamethoxazole by magnetic biochar: Effects of pH, ionic strength, natural organic matter and 17 α -ethinylestradiol. *Sci. Total Environ.* **2018**, *628–629*, 722–730. [[CrossRef](#)] [[PubMed](#)]
47. Ahmed, M.B.; Zhou, J.L.; Ngo, H.H.; Guo, W.; Johir, M.A.H.; Sornalingam, K. Single and competitive sorption properties and mechanism of functionalized biochar for removing sulfonamide antibiotics from water. *Chem. Eng. J.* **2017**, *311*, 348–358. [[CrossRef](#)]
48. Xie, M.; Chen, W.; Xu, Z.; Zheng, S.; Zhu, D. Adsorption of sulfonamides to demineralized pine wood biochars prepared under different thermochemical conditions. *Environ. Pollut.* **2014**, *186*, 187–194. [[CrossRef](#)]
49. Bedia, J.; Monsalvo, V.M.; Rodriguez, J.J.; Mohedano, A.F. Iron catalysts by chemical activation of sewage sludge with FeCl₃ for CWPO. *Chem. Eng. J.* **2017**, *318*, 224–230. [[CrossRef](#)]
50. Sevilla, M.; Ferrero, G.A.; Fuertes, A.B. Beyond KOH activation for the synthesis of superactivated carbons from hydrochar. *Carbon* **2017**, *114*, 50–58. [[CrossRef](#)]
51. Rosas, J.M.; Bedia, J.; Rodríguez-Mirasol, J.; Cordero, T. HEMP-derived activated carbon fibers by chemical activation with phosphoric acid. *Fuel* **2009**, *88*, 19–26. [[CrossRef](#)]
52. Rey, A.; Zazo, J.A.; Casas, J.A.; Bahamonde, A.; Rodriguez, J.J. Influence of the structural and surface characteristics of activated carbon on the catalytic decomposition of hydrogen peroxide. *Appl. Catal. A* **2011**, *402*, 146–155. [[CrossRef](#)]
53. Çalışkan, E.; Göktürk, S. Adsorption characteristics of sulfamethoxazole and metronidazole on activated carbon. *Sep. Sci. Technol.* **2010**, *45*, 244–255. [[CrossRef](#)]
54. Román, S.; Nabais, J.M.V.; Ledesma, B.; González, J.F.; Laginhas, C.; Titirici, M.M. Production of low-cost adsorbents with tunable surface chemistry by conjunction of hydrothermal carbonization and activation processes. *Microporous Mesoporous Mater.* **2013**, *165*, 127–133. [[CrossRef](#)]
55. Ghouma, I.; Jeguirim, M.; Dorge, S.; Limousy, L.; Ghimbeu, C.M.; Ouederni, A. Activated carbon prepared by physical activation of olive stones for the removal of NO₂ at ambient temperature. *C. R. Chim.* **2015**, *18*, 63–74. [[CrossRef](#)]
56. Jeder, A.; Sanchez-Sanchez, A.; Gadonneix, P.; Masson, E.; Ouederni, A.; Celzard, A.; Fierro, V. The severity factor as a useful tool for producing hydrochars and derived carbon materials. *Environ. Sci. Pollut. Res.* **2018**, *25*, 1497–1507. [[CrossRef](#)] [[PubMed](#)]
57. Trubetskaya, A.; Grams, J.; Leahy, J.J.; Johnson, R.; Gallagher, P.; Monaghan, R.F.D.; Kwapinska, M. The effect of particle size, temperature and residence time on the yields and reactivity of olive stones from torrefaction. *Renew. Energy* **2020**, *160*, 998–1011. [[CrossRef](#)]
58. Magalhaes, D.; Gürel, K.; Matsakas, L.; Christakopoulos, P.; Pisano, I.; Leahy, J.J.; Kazanç, F.; Trubetskaya, A. Prediction of yields and composition of char from fast pyrolysis of commercial lignocellulosic materials, organosolv fractionated and torrefied olive stones. *Fuel* **2021**, *289*, 119862. [[CrossRef](#)]

59. Parshetti, G.K.; Liu, Z.; Jain, A.; Srinivasan, M.P.; Balasubramanian, R. Hydrothermal carbonization of sewage sludge for energy production with coal. *Fuel* **2013**, *111*, 201–210. [[CrossRef](#)]
60. Wiedner, K.; Naisse, C.; Rumpel, C.; Pozzi, A.; Wieczorek, P.; Glaser, B. Chemical modification of biomass residues during hydrothermal carbonization—What makes the difference, temperature or feedstock? *Org. Geochem.* **2013**, *54*, 91–100. [[CrossRef](#)]
61. Puig-Gamero, M.; Esteban-Arranz, A.; Sanchez-Silva, L.; Sánchez, P. Obtaining activated biochar from olive stone using a bench scale high-pressure thermobalance. *J. Environ. Chem. Eng.* **2021**, *9*, 105374. [[CrossRef](#)]
62. Purnomo, C.W.; Castello, D.; Fiori, L. Granular activated carbon from grape seeds hydrothermal char. *Appl. Sci.* **2018**, *8*, 331. [[CrossRef](#)]
63. Xu, S.; Chen, J.; Peng, H.; Leng, S.; Li, H.; Qu, W.; Hu, Y.; Li, H.; Jiang, S.; Zhou, W.; et al. Effect of biomass type and pyrolysis temperature on nitrogen in biochar, and the comparison with hydrochar. *Fuel* **2021**, *291*, 120128. [[CrossRef](#)]
64. Worch, E. *Adsorption Technology in Water Treatment. Fundamentals, Processes, and Modelling*; De Gruyter: Berlin, Germany; Boston, MA, USA, 2012; ISBN 978-3-11-024022-1.
65. Ferrentino, R.; Ceccato, R.; Marchetti, V.; Andreottola, G.; Fiori, L. Sewage sludge hydrochar: An option for removal of methylene blue from wastewater. *Appl. Sci.* **2020**, *10*, 3445. [[CrossRef](#)]
66. Bajpai, A.K.; Rajpoot, M.; Mishra, D.D. Studies on the correlation between structure and adsorption of sulfonamide compounds. *Colloids Surf. A* **2000**, *168*, 193–205. [[CrossRef](#)]
67. Tonucci, M.C.; Gurgel, L.V.A.; de Aquino, S.F. Activated carbons from agricultural byproducts (pine tree and coconut shell), coal, and carbon nanotubes as adsorbents for removal of sulfamethoxazole from spiked aqueous solutions: Kinetic and thermodynamic studies. *Ind. Crops Prod.* **2015**, *74*, 111–121. [[CrossRef](#)]